Supplementary Materials

Effects of Lean Zones on SAGD Performance

Jinze Xu, Zhangxin Chen, Xiaohu Dong and Wei Zhou

In the supplementary material for the manuscript of "Effects of Lean Zones on SAGD Performance", the analytical model and detailed discussions for the effects of single-layer lean zones with different locations (above injector, between injector and producer, and below producer) on SAGD performance are demonstrated.

S1. Analytical Model

As a large amount of mobile water exists in the lean zones of oil sands reservoirs, the analytical model considering mobile water can assist in the study of the mechanism on how lean zones affect SAGD performance. In 1981, Butler proposed a theory on the prediction of heavy oil and bitumen production [S1]. In 1991, Butler further obtained the transient expression for temperature distribution during SAGD production [S2]. In 2011, Sharma obtained the results for the expressions of conductive and convective heat fluxes based on a quasi-steady-state assumption and a simplified Carslaw and Jaeger's equation [S3]. In 2013, Irani and Sahar modified Sharma's result, obtained the velocity of the condensate, and updated the expression of heat flux [S4]. In 2013, Irani and Gates took the outflow convection into consideration and modified the heat flux equations [S5]. In 2015, Ji et al coupled the thermal expansion of connate water into the expression of heat flux [S6]. However, the role of the initial mobile water and time effect has not been studied in previous analytical models [S1–S6]. We also perform the analytical study as shown in the Supplementary Material.

Owing to a large volume of mobile water in lean zones, the effect of mobile water on SAGD performance must be discussed first, to understand the effect of lean zones on such a performance. Analytical modelling is a good way to understand such an effect in homogeneous porous media. A previous understanding of the role of mobile water in SAGD performance is fully dependent on steady state flow. A transient solution is generated to explore the mechanisms of SAGD production in oil-sand reservoirs with mobile water changes in time.

The analytical solutions presented in this section have prompted the current steady single-phase analytical method to become transient, with two-phase and free water saturation. In the analytical model, the outflow convection is omitted, but is considered in the numerical model [S7,S8].

S1.1. Methodology

The coordinate is as shown in Figure S1, which is widely adopted for current studies of SAGD performance (Butler, 1991 [S1]; Sharma and Gates, 2011 [S3]; Irani and Gates, 2013 and 2014 [S5,S9]; Ji et al., 2015 [S6]). Under the assumption of a constant steam chamber growth rate U_x, the x-coordinate is transformed to the coordinate relative to the moving steam chamber interface by introducing the variable ε, which is defined as follows:

$$\varepsilon = x - \int_0^t U_x \, dt = x - U_x t \tag{S1}$$

where ε is the normal distance to the advancing front of the steam chamber, m; and U_x is the growth rate of the steam chamber, m/s.

In this model, the initial reservoir pressure is equal to P_r and the steam pressure is equal to P_{st}. The pressure variation for the water phase normal to the chamber interface can be formulated as follows [S9]:

$$c_R S_w \phi \frac{\partial P}{\partial t} = \frac{K k_{rw}}{\mu_w} \frac{\partial^2 P}{\partial x^2} \tag{S2}$$

where P is the pressure, Pa; c_R is the rock compressibility, Pa^{-1}; S_w is the water saturation, dimensionless; ϕ is the porosity, dimensionless; K is the permeability, m^2; k_{rw} is the relative permeability of water, dimensionlss; and μ_w is the dynamic viscosity of water, Pa · s.

We define the dimensionless pressure (P^*) as follows [S1]:

$$P^* = \frac{P - P_r}{P_{st} - P_r} \tag{S3}$$

where P^* is the dimensionless pressure, dimensionless; P_r is initial reservoir pressure, Pa; and P_{st} is the steam pressure, Pa.

We define the pressure coefficient as follows:

$$\omega = \frac{Kk_{rw}}{c_R S_w \phi \mu_w} \tag{S4}$$

where ω is the pressure coefficient, m^2/s.

By coupling Equations (S1)–(S4), we can obtain the equation of pressure variation as follows:

$$\frac{\partial P^*}{\partial t} = \omega \frac{\partial^2 P^*}{\partial \varepsilon^2} + U_x \frac{\partial P^*}{\partial \varepsilon} \tag{S5}$$

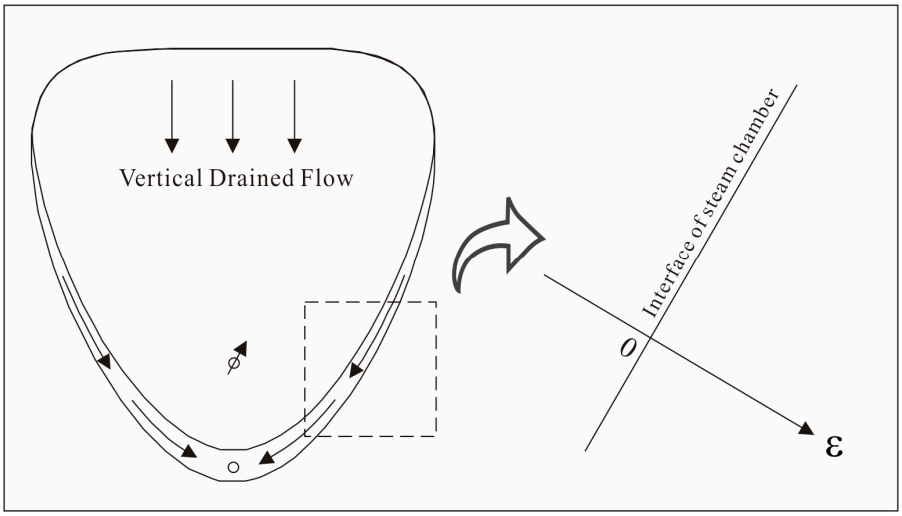

Figure S1. Scheme of analytical modelling (ε is the normal distance to the advancing front of steam chamber, m).

The boundary condition is coupled, and we acquire the following equation on the basis of the transformation of coordinates:

$$\begin{cases} \dfrac{\partial P^*}{\partial t} = \omega \dfrac{\partial^2 P^*}{\partial \varepsilon^2} + U_x \dfrac{\partial P^*}{\partial \varepsilon} \\ P^*(\varepsilon, 0) = 0 \\ P^*(0, t) = 1 \\ \dfrac{dP^*}{d\varepsilon}(\infty, t) = 0 \end{cases} \tag{S6}$$

Equation S6 is then solved. We can generate the following solution for P^* [S10]:

$$P^* = \frac{1}{2} erfc\left(\frac{\varepsilon + U_x t}{2\sqrt{\omega t}}\right) + \frac{1}{2} exp\left(-\frac{U_x \varepsilon}{w}\right) erfc\left(\frac{\varepsilon - U_x t}{2\sqrt{\omega t}}\right) \tag{S7}$$

By coupling Equations (S3) and (S7), we obtain the expression for pressure as follows:

$$P = \frac{(P_{st} - P_r)}{2}\left[erfc\left(\frac{\varepsilon + U_x t}{2\sqrt{\omega t}}\right) + exp\left(-\frac{U_x}{\varepsilon}\right) erfc\left(\frac{\varepsilon - U_x t}{2\sqrt{\omega t}}\right)\right] + P_r \tag{S8}$$

The calculation of the velocity of water (V_w) follows Darcy's law [S9]:

$$V_w = -\frac{Kk_{rw}}{\mu_w}\nabla P \tag{S9}$$

where V_w is the velocity of water, m/s.

By coupling Equations (S8) and (S9), the expression for the velocity of water can be obtained as follows:

$$V_w = -\frac{Kk_{rw}(P_{st}-P_r)}{2\mu_w}\left\{\frac{U_x[\frac{erf(\varepsilon-U_xt)}{2\sqrt{t\omega}}-1]}{exp(\frac{U_x\varepsilon}{\omega})} - \frac{\exp[-(\varepsilon-U_xt)^2]\cdot\exp\left(-\frac{U_x\varepsilon}{\omega}\right)}{\sqrt{\pi t\omega}} - \frac{\exp[-\left(\frac{\varepsilon+U_xt}{2}\right)^2/(t\omega)]}{\sqrt{\pi t\omega}}\right\} \tag{S10}$$

We apply Corey's equation to calculate k_{rw} as follows [S7]:

$$k_{rw} = (\frac{S_w - S_{wc}}{1-S_{wc}-S_{or}})^2 \tag{S11}$$

where S_{wc} is the connate water saturation, dimensionless; S_{or} is the residual oil saturation, dimensionless.

We further perform the study of the heat transfer of water with focus on the heat flux based on the transient expression of temperature distribution from Butler in 1991. Temperature is expressed as follows [S2]:

$$T = \frac{(T_{st}-T_r)}{2}\left[erfc\left(\frac{\varepsilon^*+t^*}{2\sqrt{t^*}}\right) + exp(-\varepsilon^*)\,erfc\left(\frac{\varepsilon^*-t^*}{2\sqrt{t^*}}\right)\right] + T_r \tag{S12}$$

$$\varepsilon^* = \frac{U_x\varepsilon}{\propto} \tag{S13}$$

$$t^* = \frac{U_x^2 t}{\propto} \tag{S14}$$

where T_r is the initial reservoir temperature, K; T_{st} is the steam temperature, K; $\propto$ is the reservoir diffusivity, m^2/s; t^* is the dimensionless time, dimensionless; and ε^* is the dimensionless normal distance to the advancing front of steam chamber.

The convective heat flux of water (Q_{convec}) is obtained as follows [S4–S6,S7]:

$$Q_{convec} = C_w(T-T_r)\rho_w V_w \tag{S15}$$

where Q_{convec} is the convective heat flux, $W/(m\cdot s)$; ρ_w is the density of water, kg/m^3; C_w is the water heat capacity, $J/(kg\cdot K)$; and V_w is the velocity of water, m/s.

The conductive heat flux of water (Q_{conduc}) is as follows [S4,S5]:

$$Q_{conduc} = -\kappa_T\nabla T \tag{S16}$$

where Q_{conduc} is the conductive heat flux, $W/(m\cdot s)$; and κ_T is the thermal conductivity of formation, $J/(m\cdot s\cdot K)$.

For the thermal conductivity of formation κ_T, we perform the following calculation [S6]:

$$\kappa_T = (1-\phi)\kappa_R + \phi S_w\kappa_w + \phi S_o\kappa_o \tag{S17}$$

where κ_T is the thermal conductivity of formation, $J/(m\cdot s\cdot K)$; κ_R is the thermal conductivity of rock, $J/(m\cdot s\cdot K)$; κ_w is the thermal conductivity of water, $J/(m\cdot s\cdot K)$; κ_o is the thermal conductivity of water, $J/(m\cdot s\cdot K)$; and S_o is the oil saturation, dimensionless.

By coupling Equations S12-S17, we can obtain the following equations for the convective heat flux, conductive heat flux, total heat flux and percentage of convective heat flux in the total heat flux:

$$Q_{convec} = \frac{\rho_w C_w (T_{st} - T_r)}{2}\left[erfc\left(\frac{\varepsilon^* + t^*}{2\sqrt{t^*}}\right) + exp(-\varepsilon^*)\, erfc\left(\frac{\varepsilon^* - t^*}{2\sqrt{t^*}}\right)\right] V_w \tag{S18}$$

$$Q_{conduc} = -\kappa_T[\exp(-\varepsilon^*)\left(\mathrm{erf}\left(\frac{\varepsilon^* - t^*}{2\sqrt{t^*}}\right) - 1\right) - \frac{\exp\left(-\left(\frac{(\varepsilon^* + t^*)}{2\sqrt{t^*}}\right)^2\right)}{\sqrt{\pi t^*}} - \frac{\exp(-\varepsilon^*) \cdot \exp(-\left(\frac{(\varepsilon^* - t^*)}{2\sqrt{t^*}}\right)^2)}{\sqrt{\pi t^*}}] \tag{S19}$$

$$Q_{total} = Q_{convec} + Q_{conduc} \tag{S20}$$

$$\theta = \frac{Q_{convec}}{Q_{total}} \times 100\% \tag{S21}$$

where θ is the percentage of convective heat flux in the total heat flux, dimensionless.

S1.2. Results and Discussion

We use the data presented in Table S1 to evaluate the effect of mobile water. In order to validate our analytical model, CMG STARS is used to predict the mass and heat transfer ahead of the steam chamber edge in the SAGD numerical model with a grid size of 0.5 m, by employing the same parameters as those in Table S1. A comparison of the pressure and temperature profiles of the two models is as shown in Figure S2. For the results from the analytical and numerical model, the pressure and temperature profiles are quite similar. As the result in the numerical model is taken from the average of the values in a block, the analytical result is much smoother and and more accurate. The water velocity is important for water production and convective heat flux. Figure S3(a) implies that with increasing time, the wave crest begins to move in the direction of the external normal line of the steam chamber surface. The water velocity also decreases with time. After five years, the water velocity hardly changes and begins to be steady. Due to the high water effective permeability, a high water saturation leads to a high water velocity, as Figure S3(b) shows. We further study the heat transfer under a water saturation of 0.5. According to Figure S4(a), temperature changes significantly during the first five years. After five years, the temperature distribution begins to stabilize. Figure S4(b) implies that the total heat flux also tends to be steady after five years. As the temperature does not increase significantly after one year, the heat needed also decreases.

As Figure S5(a) shows, the convective heat flux decreases with time. Such a reduction is due to the decrease in the water velocity, as shown in Figure S5(b). Coinciding with the trend of temperature with time, the conductive heat flux also tends to be steady after five years, as Figure S6(a) shows. The conductive heat flux fully depends on the temperature gradient under certain water saturation. As the temperature gradient decreases, the conductive heat flux needed also decreases over the 10 years. According to Figure S6(b), the convective heat flux dominates the total heat flux. However, with the decrease in the water velocity after one year, the convective heat flux needed also decreases and tends to be steady after five years. In fact, water saturation plays a significant role in the heat flux. Considering that the heat flux tends to be steady after five years, we select the time of five years to study the effect of mobile water. As shown in Figure S7(a), the total heat flux needed for SAGD production increases with an increase in water saturation. Such an increase is mainly caused by an increase in the convective heat flux, as Figures S7(b) to S7(d) show. The increase in the convective heat flux is greatly affected by an increase in the water velocity (Figure S5(b)).

Table S1. Reservoir Parameters in the Model.

Parameters	Value
Connate Water Saturation, dimensionless	0.2
Residual Oil Saturation, dimensionless	0.2
Rock Compressibility, Pa^{-1}	1×10^{-10}
Initial Porosity, dimensionless	0.3
Velocity of the Edge of Steam Chamber, m/s	1.74×10^{-7}
Density of Water, kg/m^3	1000
Viscosity of Water, $Pa \cdot s$	1×10^{-3}
Reservoir Thermal Conductivity, $W/(m \cdot ℃)$	1.45
Heat Capacity of Water, $J/(kg \cdot ℃)$	4200
Permeability, m^2	9.87×10^{-12}
Injection Pressure, Pa	2×10^7
Reservoir Initial Pressure, Pa	1.05×10^7

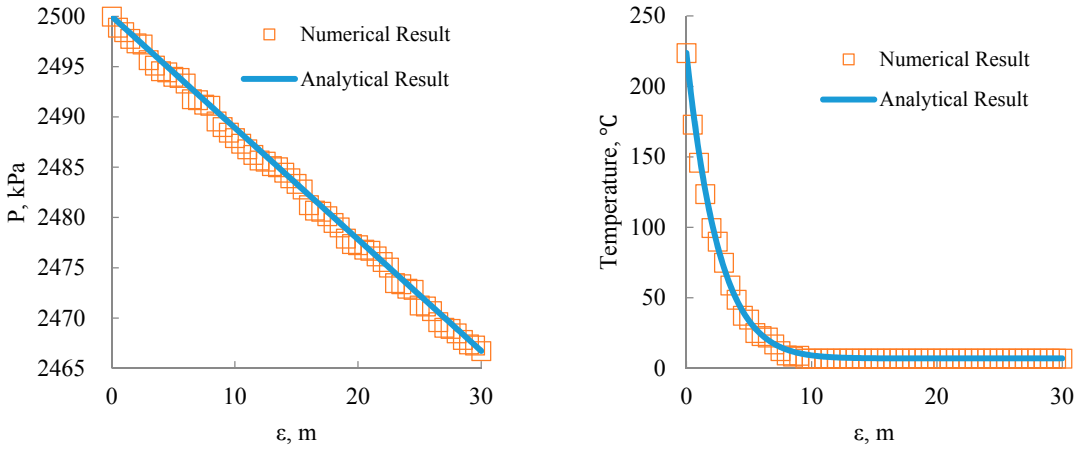

(**a**) (**b**)

Figure S2. Validation between analytical model and numerical model (a: relationship between normal distance to the advancing front of steam chamber and pressure; b: relationship between normal distance to the advancing front of steam chamber and temperature).

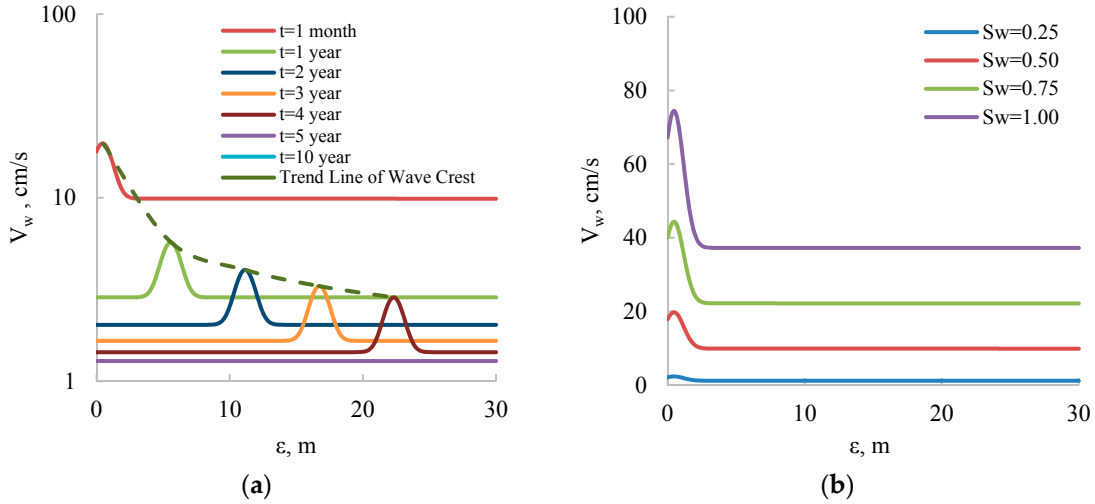

Figure S3. Profile of water velocity (a: relationship between the normal distance to the advancing front of steam chamber and the water velocity at different times, S_w=0.5; b. relationship between the normal distance to the advancing front of steam chamber and the water velocity at different water saturations, t= 1 month).

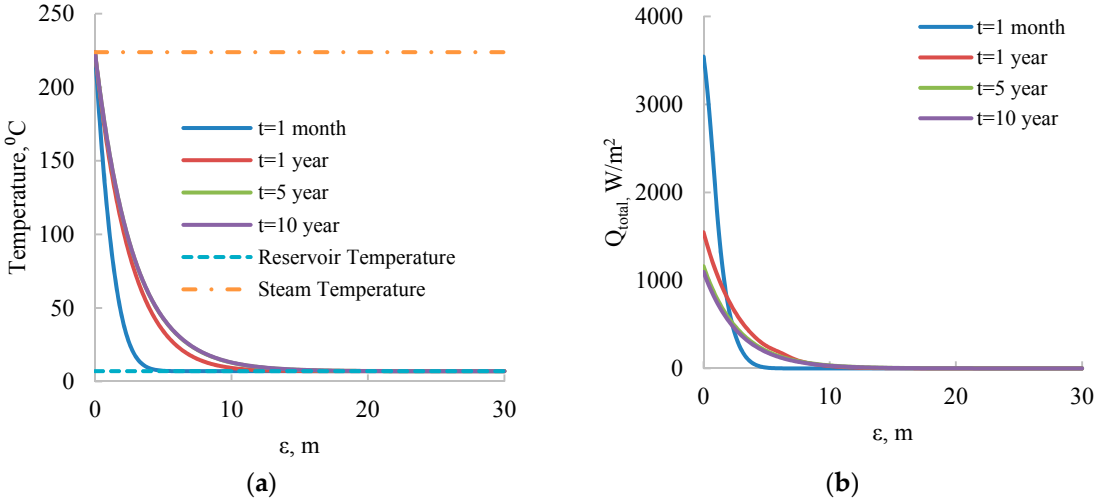

Figure S4. Profile of temperature and total heat flux at different times, S_w=0.5 (a. relationship between the normal distance to the advancing front of steam chamber and the temperature; b: relationship between the normal distance to the advancing front of steam chamber and the total heat flux).

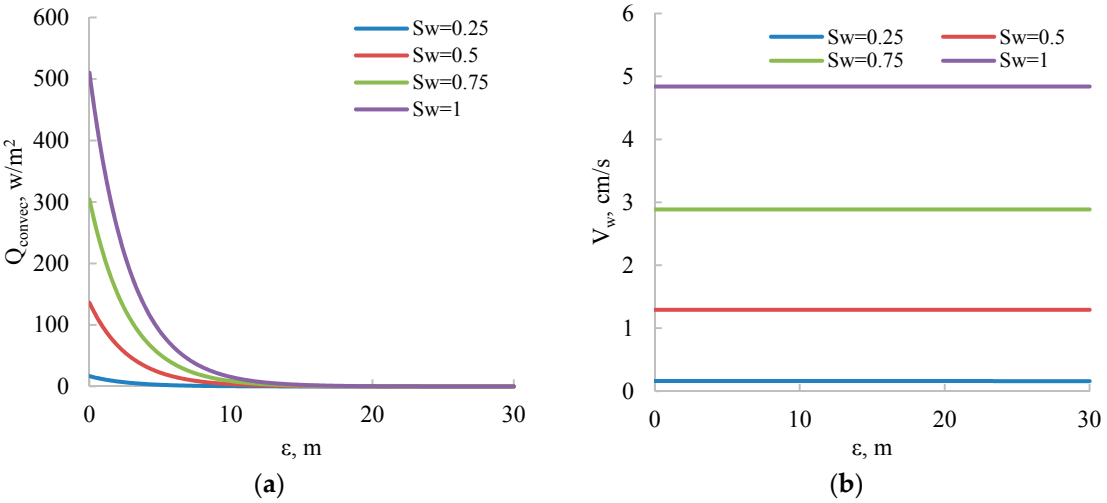

Figure S5. Profile of convective heat flux and water saturation at different water saturations, t=5 year (a: relationship between the normal distance to the advancing front of steam chamber and the convective heat flux; b: relationship between the normal distance to the advancing front of steam chamber and the water velocity).

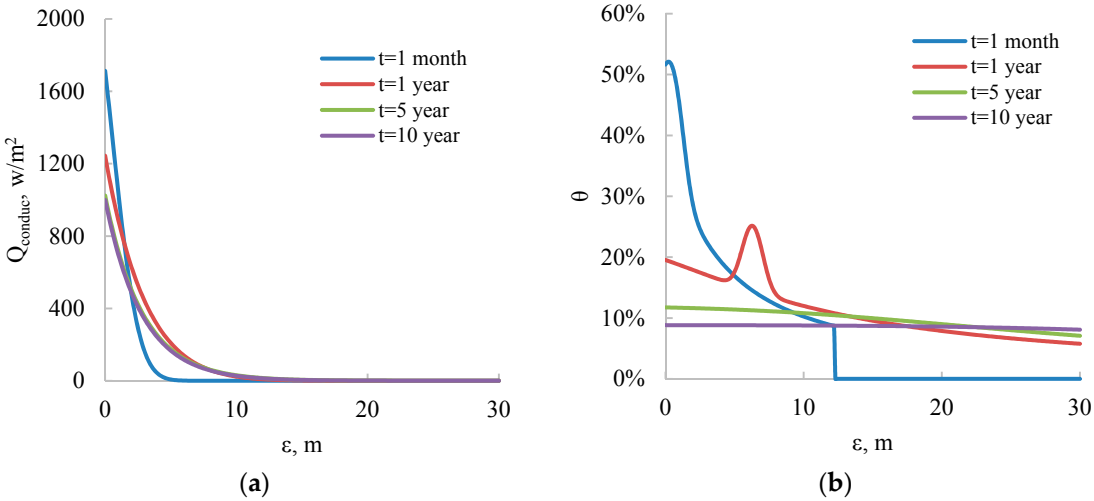

Figure S6. Profile of conductive heat flux and percentage of convective heat flux at different times, S_w=0.5 (a: relationship between the normal distance to the advancing front of steam chamber and the conductive heat flux; b: relationship between the normal distance to the advancing front of steam chamber and the percentage of convective heat flux).

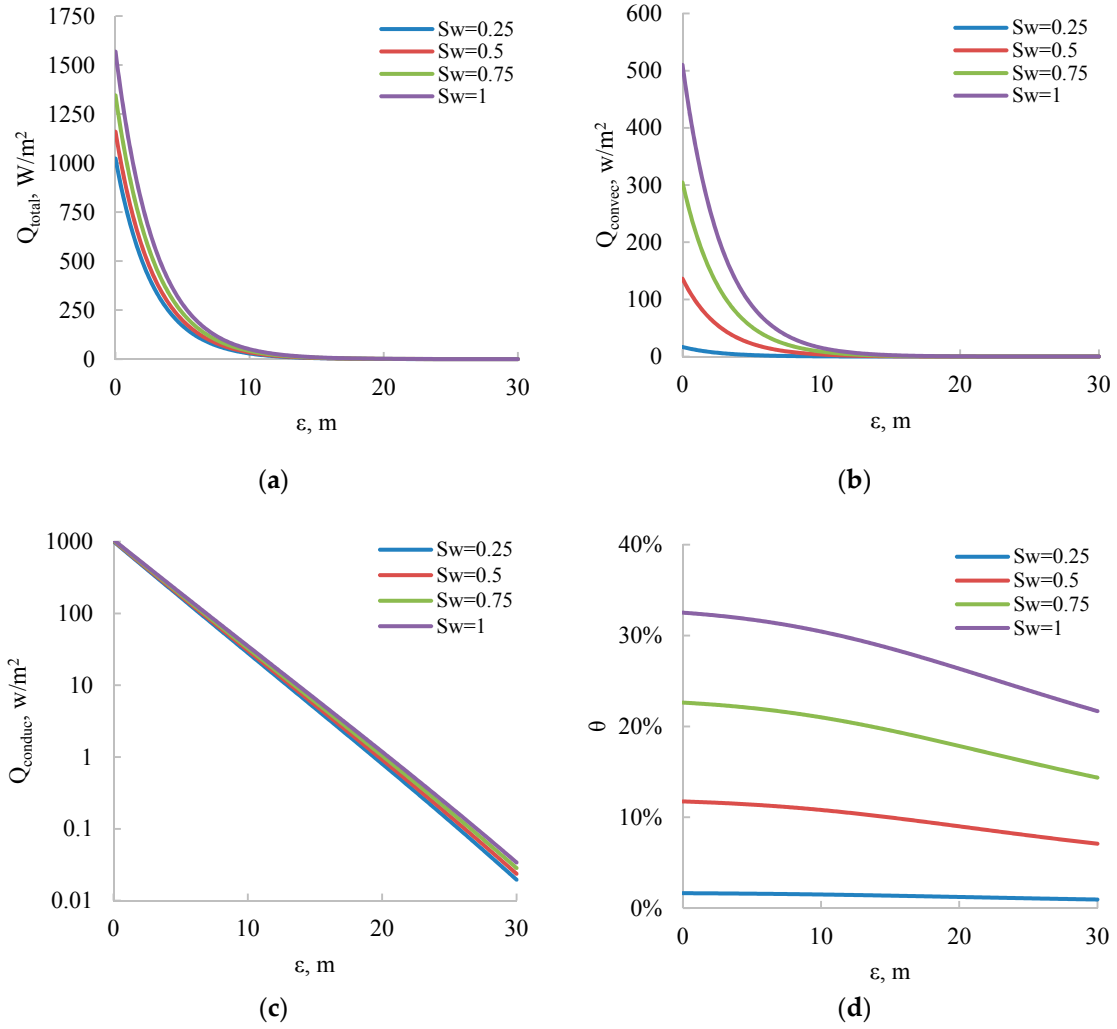

Figure S7. Profile of total heat flux, convective heat flux, conductive heat flux and the percentage of convective heat flux at different water saturations, t = 5 year (a: relationship between the normal distance to the advancing front of steam chamber and the total heat flux; b: relationship between the normal distance to the advancing front of steam chamber and the convective heat flux; c: relationship between the normal distance to the advancing front of steam chamber and the conductive heat flux; d: relationship between the normal distance to the advancing front of steam chamber and the percentage of convective heat flux).

S2. Single-Layer Lean Zones with Different Locations

Effects of single-layer lean zones with different locations on SAGD performance are as follows:

(1) AI Type: The results for SOR and SCV are shown in Figures S8 and S9. These results agree with the case (11 3 2.5; size, 11 m; interval distance, 3 m; thickness, 2.5 m) in which the largest size and thickness but the smallest interval distance yield the highest steam chamber volume (SCV) and steam-oil ratio (SOR) (i.e., 13435.25 m^3 and 3.143875, respectively). For the case (3 13 0.5), SCV and SOR decrease to 13143.92 m^3 and 3.007215 m^3/m^3, respectively. A large thickness, large size, and small interval distance lead to a large SCV. As water provides the priority pathway for steam, this enables the steam to go far and high. Thus the injectivity of the injector increases. Under the same pressure, substantial steam can be injected for the case with lean zones. For both the SOR and SCV, the thickness dominates (Figures S10 and S11).

(2) BIP Type: According to Figures S12 and S13, the relationship among SOR, SCV, and the three parameters for the BIP type is the same as that for the AI type. For the SAGD production with the single-layer lean zone, a large thickness, large size, and small interval distance result in large SOR

and SCV values. The analysis of the main effects shows that thickness remains the key parameter for SOR and SCV (Figures S14 and S15)

(3) BP Type: For SOR, the trend is the same as shown in Figure S16. Specifically, because the lean zone does not locate in the steam chamber, the large thickness, large size, and small interval distance lead to substantial water production under the same steam trap. Figure S17 shows that SCV is not highly dependent on thickness, size, and interval distance as the lean zone below the producer is not inside the steam chamber in the BP case.

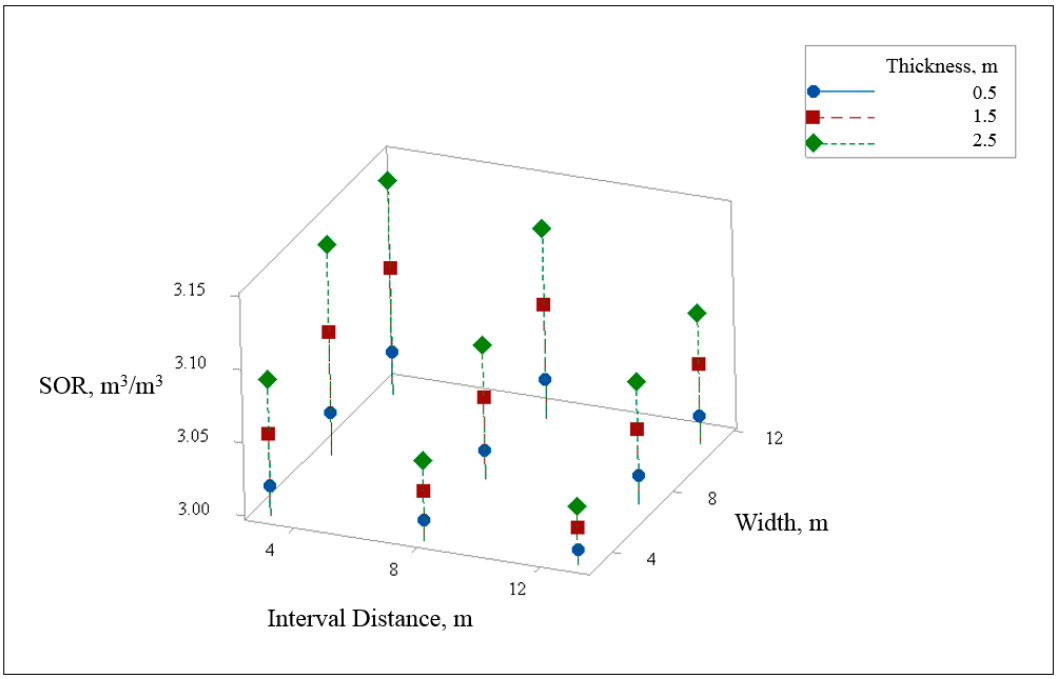

Figure S8. Relationship between width, interval distance, thickness and SOR (AI case).

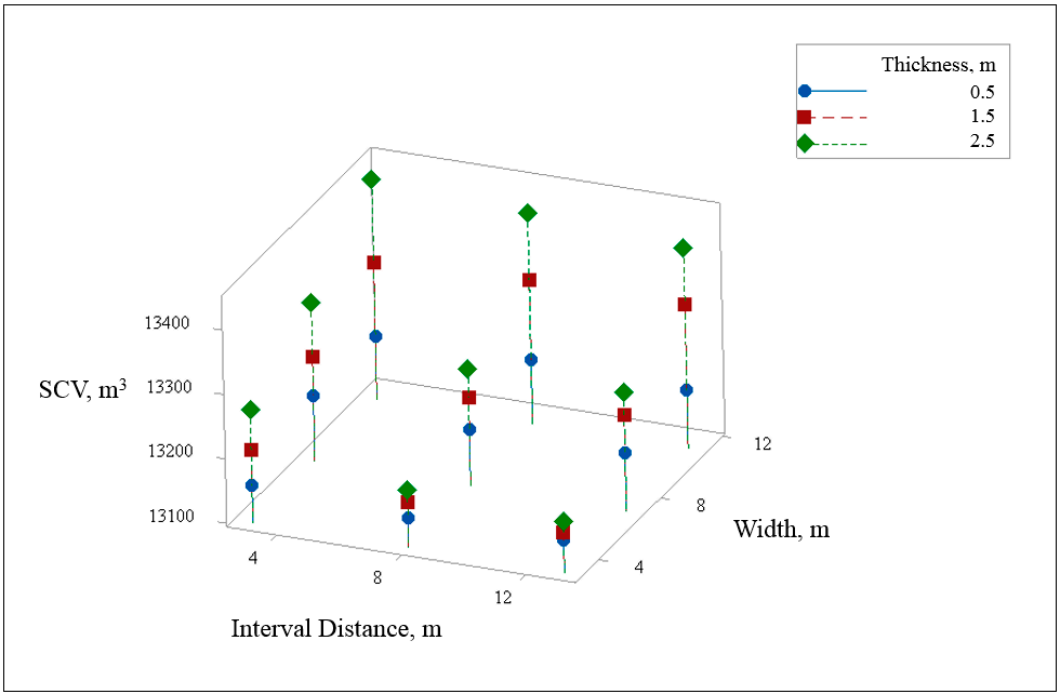

Figure S9. Relationship between width, interval distance, thickness and SCV (AI case).

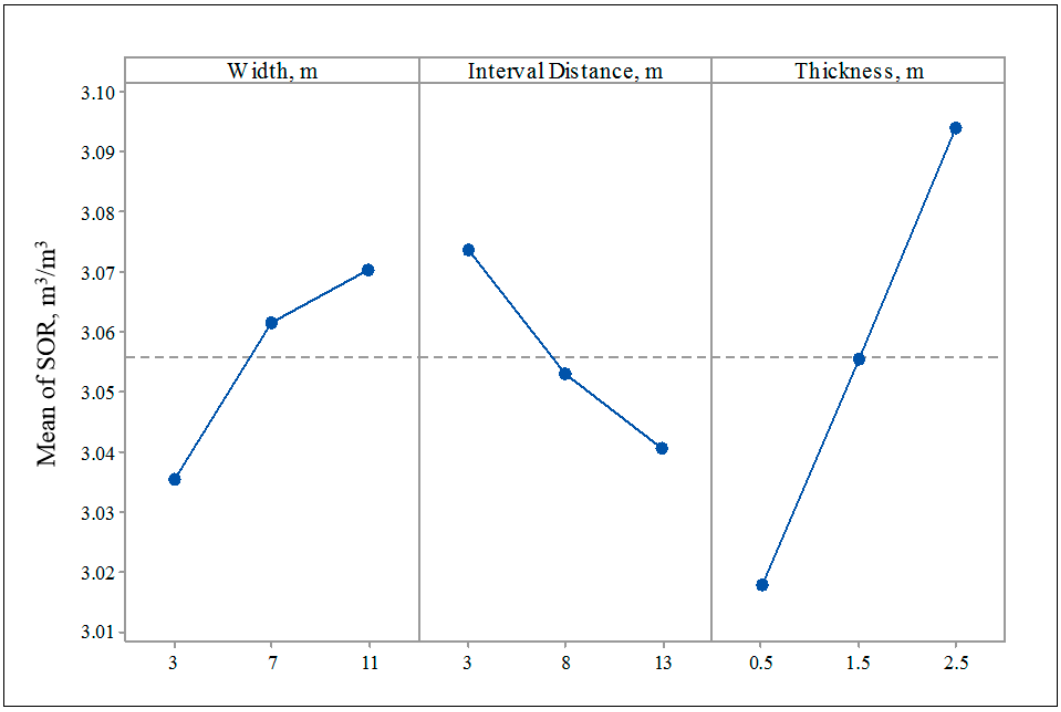

Figure S10. Main effect analysis for SOR (AI case).

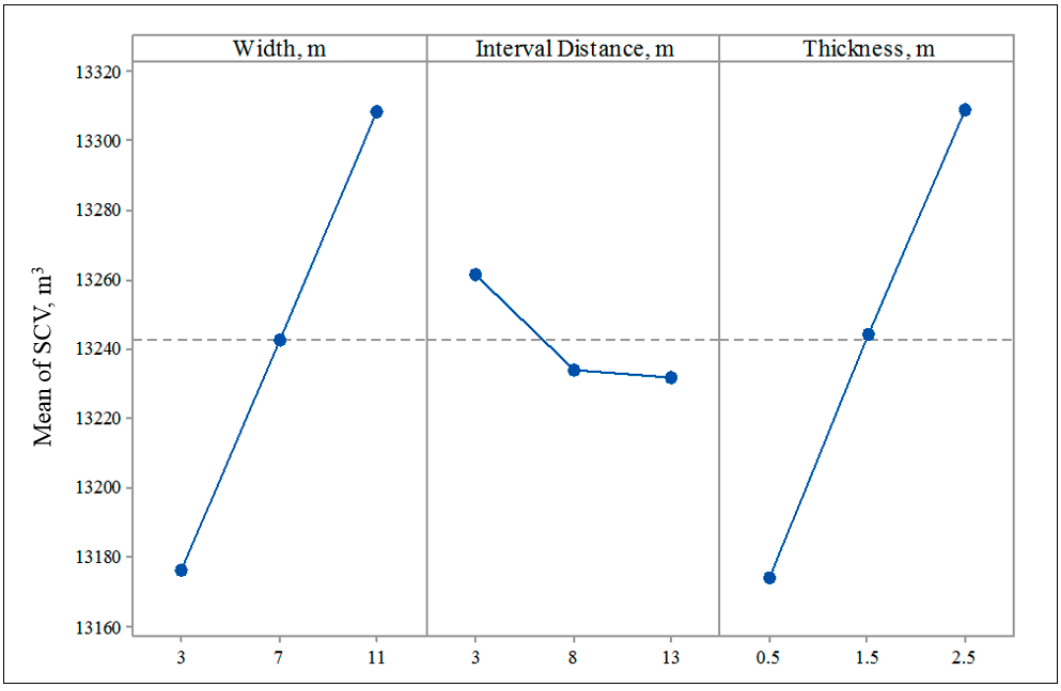

Figure S11. Main effect analysis for SCV (AI case).

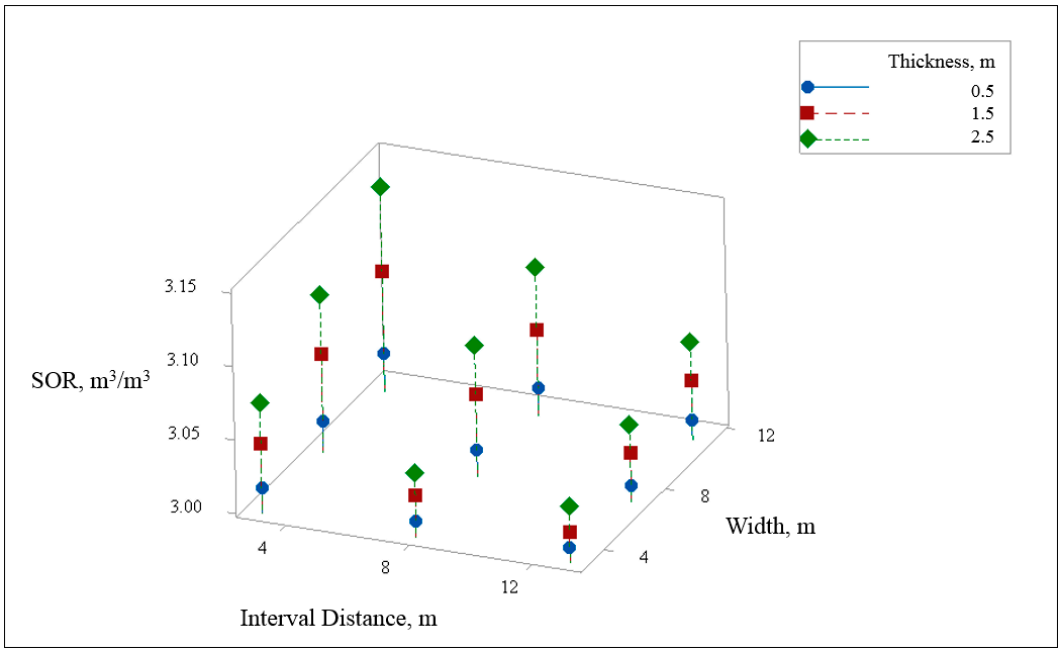

Figure S12. Relationship between width, interval distance, thickness and SOR (BIP case).

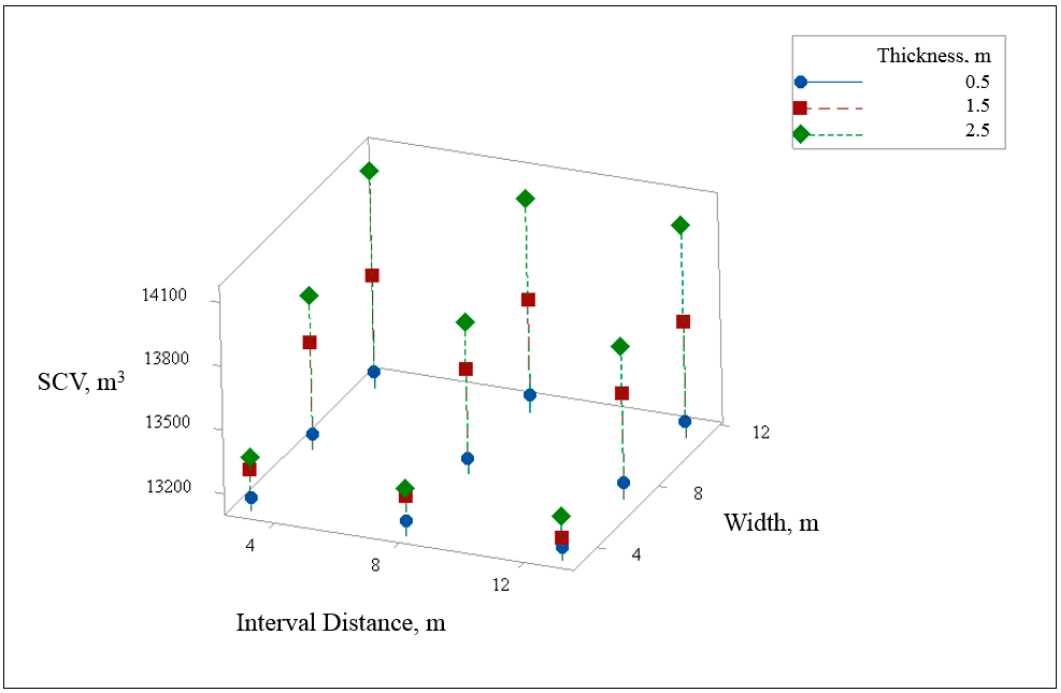

Figure S13. Relationship between width, interval distance, thickness and SCV (BIP case).

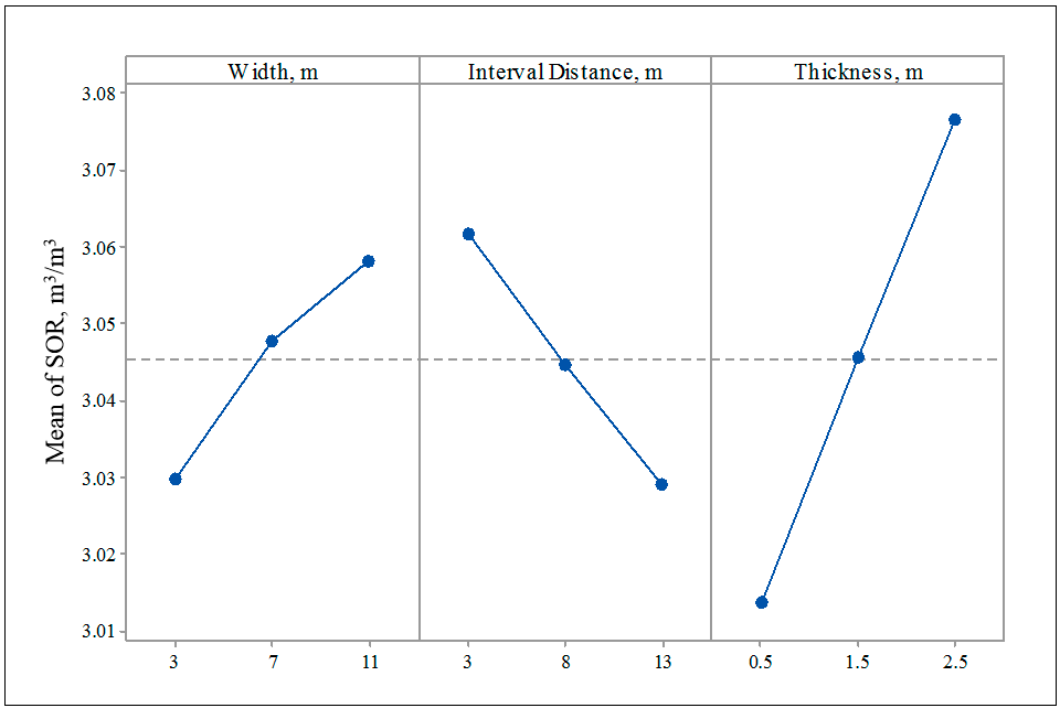

Figure S14. Main effect analysis for SOR (BIP case).

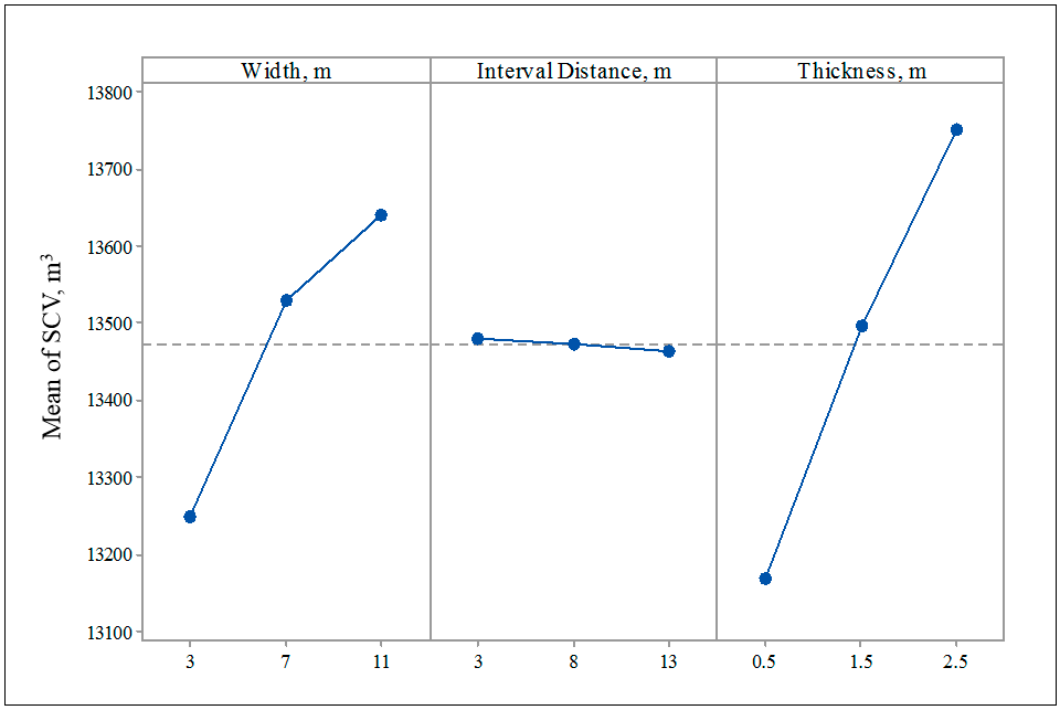

Figure S15. Main effect analysis for SCV (BIP case).

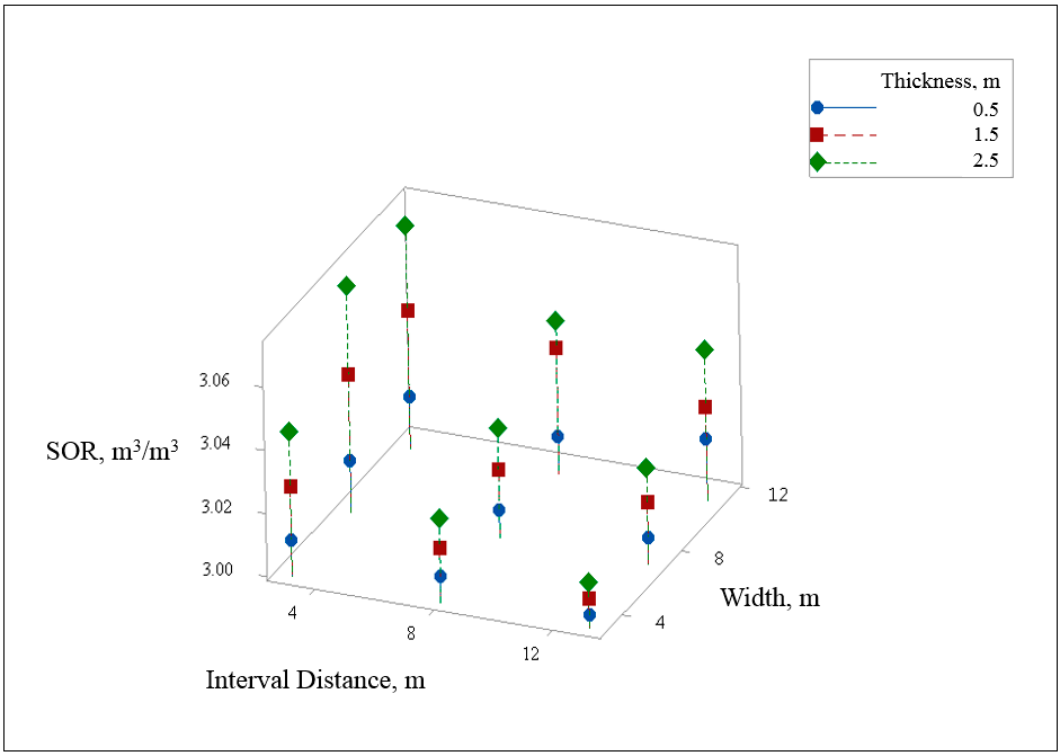

Figure S16. Relationship between width, interval distance, thickness and SOR (BP case).

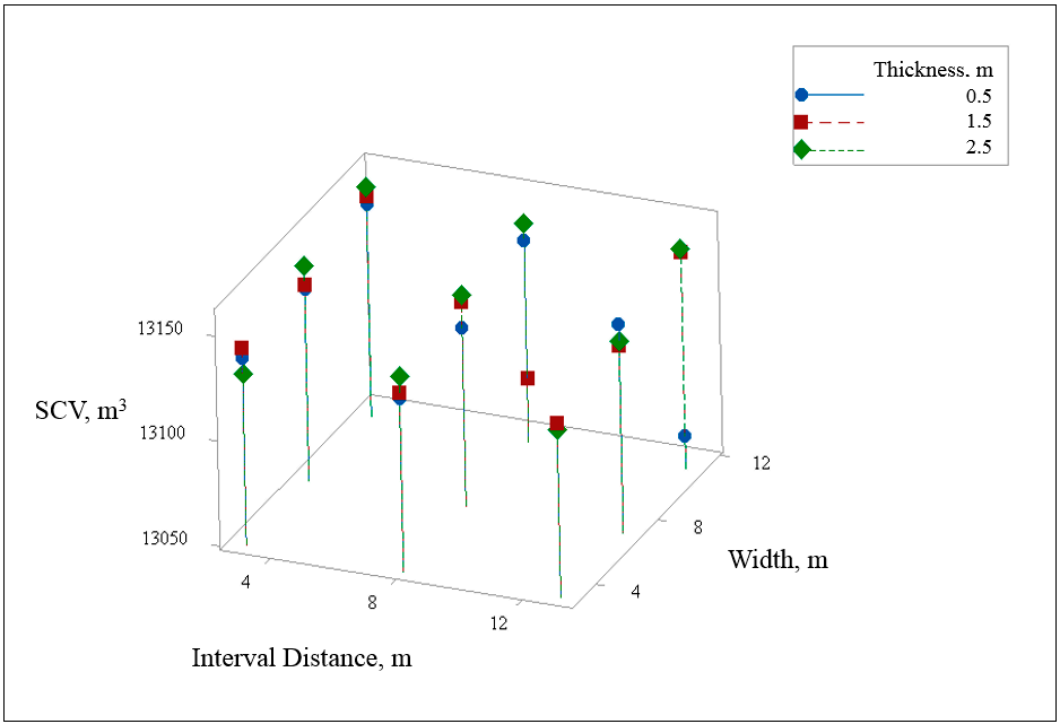

Figure S17. Relationship between width, interval distance, thickness and SCV (BP case).

Supplementary Abbreviations

The following abbreviations are used in this supplementary material:

ϕ	porosity, dimensionless;
μ_w	dynamic viscosity of water, $\mathrm{Pa \cdot s}$;
$\propto$	reservoir diffusivity, $\mathrm{m^2/s}$;
ε	normal distance to the advancing front of steam chamber, m;
ρ_o	density of oil, $\mathrm{kg/m^3}$;
ρ_w	density of water, $\mathrm{kg/m^3}$;
θ	percentage of convective heat flux in the total heat flux, dimensionless;
κ_o	thermal conductivity of oil, $\mathrm{J/(m \cdot s \cdot K)}$;
κ_w	thermal conductivity of water, $\mathrm{J/(m \cdot s \cdot K)}$;
κ_R	thermal conductivity of rock, $\mathrm{J/(m \cdot s \cdot K)}$;
κ_T	thermal conductivity of formation, $\mathrm{J/(m \cdot s \cdot K)}$;
C_o	oil heat capacity, $\mathrm{J/(kg \cdot K)}$;
C_w	water heat capacity, $\mathrm{J/(kg \cdot K)}$;
c_R	rock compressibility, $\mathrm{Pa^{-1}}$;
K	permeability, $\mathrm{m^2}$;
k_{rw}	relative permeability of water, dimensionless;
P_r	initial reservoir pressure, Pa;
P_{st}	steam pressure, Pa;
P^*	dimensionless pressure;
Q_{conduc}	conductive heat flux, $\mathrm{W/(m \cdot s)}$;
Q_{convec}	convective heat flux, $\mathrm{W/(m \cdot s)}$;
Q_{total}	total heat flux, $\mathrm{W/(m \cdot s)}$;
S_o	oil saturation, dimensionless;
S_{or}	residual oil saturation, dimensionless;
S_w	water saturation, dimensionless;
S_{wc}	connate water saturation, dimensionless;
T_r	initial reservoir temperature, K;
T_{st}	steam temperature, K;
t	time, s;
t^*	dimensionless time;
U_x	velocity of the advancing front of steam chamber, m/s;
V_w	velocity of water, m/s.

Supplementary References

S1. Butler, R.M. *Thermal recovery of oil and bitumen*; Prentice Hall: Upper Saddle River, NJ, USA, 1991.

S2. Butler, R.M. Rise of interfering steam chambers. *J. Can. Petrol. Technol.* **1987**, *26*, 70–75.

S3. Sharma, J.; Gates, I.D. Convection at the edge of a steam-assisted-gravity-drainage steam chamber. *SPE J.* **2011**, *16*, 503–512.

S4. Irani, M.; Ghannadi, S. Understanding the heat-transfer mechanism in the steam-assisted gravity-drainage (SAGD) process and comparing the conduction and convecion flux in bitumen reservoirs. *SPE J.* **2013**, *18*, 134–145.

S5. Irani, M.; Gates, I.D. Understanding the convection heat-transfer mechanism in steam-assisted-gravity-drainage process. *SPE J.* **2013**, *18*, 1202–1216.

S6. Ji, D.; Zhong, H.; Dong M.; Chen, Z. Study of heat transfer by thermal expansion of connate water ahead of a steam chamber edge in the steam-assisted-gravity-drainage process. *Fuel* **2015**, *150*, 592–601.

S7. Stars, C. *Advanced Process and Thermal Reservoir Simulator*; Computer Modelling Group Ltd.: Calgary, AB, Canada, 2012.

S8. Chen, Z. *Reservoir simulation: mathematical techniques in oil recovery*; Siam: Philadelphia, PA, USA, 2007.

S9. Irani, M.; Gates, I.D. On the Stability of the Edge of a Steam-Assisted-Gravity-Drainage Steam Chamber. *SPE J.* **2014**, *19*, 280–288.

S10. Jaiswal, D.K.; Kumar, A.; Yadav, R.R. Analytical solution to the one-dimensional advection-diffusion equation with temporally dependent coefficients. *J. Water Resource Prot.* **2011**, *3*, 76–84.